Soft Matter

Volume 1 | Number 1 | Jan 2013 | Pages 1–100

Soft Matter

www.rsc.org/softmatter

ROYAL SOCIETY OF CHEMISTRY

www.rsc.org/softmatter

Snapshotted glass and gel transitions of stable colloidal dispersions after shear-driven aggregation in a microchannel

Xia Meng, Hua Wu[*] and Massimo Morbidelli[*]

Institute for Chemistry and Bioengineering,

Department of Chemistry and Applied Biosciences,

ETH Zurich, 8093 Zurich, Switzerland

_____

* Corresponding authors: Email: hua.wu@chem.ethz.ch; massimo.morbidelli@chem.ethz.ch

Abstract. Intense shear can lead to aggregation of colloids that are well stable at rest. The aggregation process typically has an induction time and then becomes explosive, leading to fast phase transitions. We study the phase evolution along the shear-driven aggregation in a short microchannel (MC) under intense shear, for a colloid with a high interaction energy barrier that ensures high stability of the particles and the clusters before and after intense shear. The short residence time allows us to snapshot the phase evolution by repeatedly cycling the colloid in the MC. It is found that, depending on the particle concentration, besides a fluid of clusters and a solid-like gel, there is another solid-like state between them: Wigner glass of clusters. Their transitions occur in a large range of the particle concentration. We have proposed a phase diagram that describes how the transitions of the three phases evolve at the aggregation steady-state in the colloidal interaction vs particle concentration plane.

1. Introduction

Colloidal dispersions with different inter-particle interactions show a variety of phase behaviour. Spherical particles with a steep repulsive potential exhibit a progressive phase transition from a fluid to a jamming state and then to a fully crystallized state as the particle volume fraction, ϕ, increases. The jamming state is a glassy state, referred to as repulsive glass or Wigner glass, which may occur in a large range of ϕ, depending on the range of the repulsion and temperature.[1-5] For strongly attractive colloids, the system arrests at relatively low particle densities (ϕ<0.2), resulting from irreversible inter-particle bonding of fractal scaling, and the arrested state is often referred to as a gel.[6] For the colloidal systems whose interaction potential is attractive at a short distance and repulsive at a long separation, such competing interactions may lead to rich hierarchical self-organization behaviour such as finite sizes of clusters,[6-16] dynamical arrest to form a Wigner glass of clusters,[16, 17] or percolation of clusters to form a gel.[14, 18]

On the other hand, even for colloids with a steep repulsive potential such that they are extremely stable at rest, proper shear forces can drive them to aggregate, leading to phase transition, if the primary (minimum) well of the interactions is deep enough.[19] Such shear-driven transition from liquid-like colloids to solid-like gels has been shown experimentally for various systems with strong DLVO (Derjaguin-Landau-Verwey-Overbeek)-type interactions.[20-27] The mechanism for the transition was proposed to be similar to that under stagnant conditions, resulting from percolation of fractal clusters at high packing fractions.[19, 23] However, a clear picture how different phases evolve and transfer along the shear-driven aggregation has not been given in the literature. Therefore, this work is dedicated to detailed investigations of the shear-driven phase evolution for a colloidal system that is strongly stabilized by surface charges and

surfactants. It will be seen that along the shear-driven aggregation process, we are able to observe progressively three phases: fluid of clusters, Wigner glass of clusters and gel. The presence of the Wigner glass of clusters evidences strong repulsion among the clusters, originating from the strong repulsion of the primary particles.

2. The shear-driven aggregation experiments

2.1 The colloidal system

We use aqueous dispersions of polystyrene particles as model colloidal systems, which were synthesized in our lab by conventional emulsion polymerization with KPS (potassium per-sulphate) as initiator and SDS (sodium dodecyl sulphate) as surfactant. The mean radius of the particles was $a = 21.5$ nm, determined by dynamic light scattering. The particles were stabilized by both fixed surface charges from polymer chain end (sulphate) groups and the surfactant (25% coverage regarding to the saturated adsorption of SDS on polystyrene surface). The zeta potential of the primary particles after removing the surfactant, measured by Zetasizer Nano (Malvern, UK) instrument at $\phi = 1.0 \times 10^{-4}$, is -45 mV. Thus, the primary particles are well stabilized with no tendency of aggregation at rest.

2.2 The shearing device and procedure

The shear-driven aggregation of the above colloid was carried out using a commercially available device, Homogenizer HC-5000 (Microfluidics), equipped with a z-shape microchannel (MC) with a rectangular cross section of ~0.05 mm^2 and length of 5.8 mm, about which details can be found elsewhere.[22] A schematic illustration of the device is given in Sketch 1. The intense shear in the MC is generated by forcing the colloid to pass through the MC under high pressure.

A pressure gauge is settled in the front of the MC inlet to measure the instantaneous pressure drop (ΔP) through the MC. The relation between the shear rate $\dot{\gamma}$ in the MC and the pressure drop ΔP, reported by the device supplier, is $\dot{\gamma}$ [1/s] = 1.02×10^4 ΔP [bar], where $\Delta P \in$ [20,150] bar. It is worth noting that the residence time of the particles or clusters in the MC is extremely short (e.g., ~27 μs at $\Delta P = 150$ bar, *i.e.*, at $\dot{\gamma} = 1.5 \times 10^6$ s^{-1}). This means that we are able to snapshot the aggregation status of a colloidal system in very short time intervals.

Moreover, when one notices that the cross section of the MC is only ~0.05 mm^2, while the cross section at its outlet is ~20 mm^2 (400 times), we can consider that the shear is immediately removed outside the MC and all the shear-driven events (aggregation, breakage and restructuring) take place only within the MC. Then, due to the strong repulsion, the Brownian motion-driven aggregation and breakage are negligible, and the formed clusters are practically 'frozen' outside the MC. Therefore, with the above features, after a dispersion passes through the MC, we can offline characterize it and then send it back to the inlet for further shearing. When we repeat such experiments for many cycles, we are able to monitor the shear-driven phase evolution.

For a typical shearing experiment, the tube connected to the MC outlet introduces the sheared dispersion directly to the chamber at the inlet such that the shearing process is continuous, as indicated in Sketch 1. The shearing time is computed by $t = 0.8 \times N_c$, where N_c is the number of pulses and 0.8 is the pumping time of each pulse in second. The shear rate is fixed at $\dot{\gamma} = 1.5 \times 10^6$ s^{-1} in this study. We explored the phase transition behavior of the shear-driven aggregation process in the range of the particle volume fraction, $\phi \in [2\%, 15\%]$.

3.   Results and discussion

3.1 Time evolution of the shear-driven process

It has been well documented[22, 25] that the shear-driven aggregation leads to clusters of bimodal distributions: the average size of the first class is not far from the primary particles, while that of the second class is orders of magnitude larger than that of the first. Thus, by centrifugation we can easily isolate the big clusters and quantify the conversion of the primary particles to the big clusters, x, which is defined as the total mass of the big clusters divided by the total mass of the initial primary particles. Then, the radius of gyration (R_g) and fractal dimension (d_f) of the big clusters can be determined by small-angle light scattering measurements.[28] Fig. 1 shows the time evolution of x, R_g and d_f in the case of $\phi = 3.0\%$. The conversion shows a sharp upturn after an induction time, which is related to the activation energy barrier, $U_{act} = U_m - 6\pi\alpha\mu\dot{\gamma}R_g^3$, of the shear-driven aggregation kinetics, $k_{1,1} \quad \sqrt{(3\pi\alpha\mu\dot{\gamma}R_g^3 - U_m'')/k_B T} \times e^{-U_{act}/k_B T}$ (α is a coefficient related to the type of flow, e.g., $\alpha = 1/3\pi$ for simple shear flow,[19] μ is the viscosity of the system, U_m is the colloidal interaction barrier, and $U_m'' < 0$ is the second derivative of U_m).[19] Since U_{act} is positive, initially, the aggregation is very slow; when a certain cluster size, $R_g = (U_m / 6\pi\alpha\mu\dot{\gamma})^{1/3}$, is reached, U_{act} vanishes and then even becomes negative, and the aggregation becomes much faster and goes with the cube of R_g in the exponent. The R_g evolution exhibits an overshoot; the maximum R_g appears just after the upturning point of x, indicating that once the critical cluster size is reached, the extremely fast aggregation rate leads to the clusters growing larger and larger in an extremely short time.[29] The fractal dimension of the clusters increases with time from $d_f = 2.4 \pm 0.05$ to 2.8 ± 0.05, suggesting occurrence of the shear-driven restructuring.[30-32]

It is evident that the size and fractal dimension of the clusters result from dynamic equilibrium among the shear-driven aggregation, breakage and restructuring.[33, 34] Initially, aggregation is dominant, and big clusters are formed in an extremely short time associated with the vanishing of the activation energy barrier. Then, as the conversion and number of clusters increase, breakage and restructuring start to play an important role. In fact, from computations of the average cluster mass (i) based on the fractal scaling, $i = k(R_g / a)^{d_f}$ with $k = 4.46 \times d_f^{-2.08}$,[35] using the measured R_g and d_f, we found that, after the R_g maximum, the region where R_g decreases with the shearing time in Fig. 1 is indeed related to not only compacting (restructuring) but also breakage of the big clusters (i.e., i decreases with time).[32] Fig. 2 shows the typical shape and morphology of the big clusters in the later stage. It is seen that the shape of the big clusters is rather irregular, and the scanning electron microscope confirms that the big clusters are very compact. After $x > 0.6$ in Fig. 1, since the primary particle concentration reduces to ~1/3 of the initial concentration, the rate of the aggregation, as a second-order process, would reduce one order of magnitude, and it follows that the increase in x with time becomes much slower. Thus, it is difficult to reach 100% conversion at low particle concentrations. This is the reason why we decided to carry out our experiments in the range of $\phi \in [2\%, 15\%]$. Note that also due to the concentration effect, the induction time decreases as ϕ increases, and it approaches zero when ϕ >5.0%. Moreover, when ϕ >15%, the system gels directly after passing through the MC just one time.

3.2 Time evolution of the phases and phase transition

As the packing fraction of the clusters increases with the conversion, at a certain point, the liquid-like state eventually transfers to a solid-like state. To have a glance of the state transition,

7

we show in the insert of Fig. 3 some pictures taken at different shearing times in the case of $\phi =$ 5.0%. It is evident that the samples in the first three pictures at $t = 0$ s, 20 s and 50 s are liquid-like, while the last two at $t = 80$ s and 180 s are solid-like. However, for the two solid-like samples when we performed dilution experiments with water,[36] the sample at $t = 80$ s can be completely dispersed after gentle shaking, while the one at $t = 180$ s cannot, keeping its shape for days. This clearly indicates that in the former the clusters are not interconnected and repel each other, while in the latter they are interconnected. Thus, the former is a Wigner glass of clusters, and the latter is a gel. Further evidence is that the scattering structure factor of the former is typical of fractal clusters, as it is shown in Fig. 4a, flat in the small q range and has only one bending (Guinier) regime. For the latter, we have to use a glass bar to mash the gel flocks and then further disperse them by mechanical agitation. Obviously, in this way, the gel and cluster structure can be significantly altered, thus not reported here. However, we found that at $t = 150$ s, the gel can still be dispersed in water by substantial stirring (without using a glass bar to mash). This indicates that at $t = 150$ s the percolation has started towards the gel but not yet completed. The obtained scattering structure factor is shown in Fig. 4b, and it has two bending regimes, characteristic of a gel,[28] one related to the clusters and another to the secondary structure made of cluster interconnection. It is therefore concluded that along the shear-driven aggregation, three states can exist: fluid of clusters, Wigner glass of clusters and gel.

The presence of the Wigner glass state is obviously related to the repulsive nature of the system, which remains even after forming clusters. The occurrence of the gel state after the glass state is different from the phase transition of repulsive spherical particles, where the glass state is followed by a fully crystallized state. This arises because of two factors: 1) for our system a strong attraction exists at the extremely short screening length, which can be reached under the

intense shear, and 2) the clusters are of irregular shape and surface. Thus, once the clusters are connected at the attraction well, it is difficult for them to relax to a crystal state.

With the visual observation and dilution experiment mentioned above, as well as light scattering characterizations, we are able to define the transitions of different phases. Note that the glass transition is typically defined in the literature as the point where the viscosity becomes larger than 10^{13} poise, or when the non-ergodic behaviour (by light scattering) persists for an observation timescale longer than 10^2 s.[37] The former is somewhat empirical, and the latter cannot be realized for our system, because at the given ϕ range, the dispersions are too turbid to perform such light scattering experiments. The obtained phase evolution diagram is shown in Fig. 3, in the form of the packing fraction of the total clusters, ϕ_c, as a function of the shearing time. The ϕ_c values are computed by $\phi_c = x\phi k^{-1}(R_g / a)^{3-d_f}$, and the x, R_g and d_f values are determined experimentally. The two broken lines are found experimentally, which divide the plane from small to large ϕ_c values into three phases: fluid of clusters, Wigner glass of clusters and gel.

In the case of the initial particle volume fraction, $\phi \leq 3\%$, the system is always liquid-like in the entire shearing time. The ϕ_c value exhibits a local maximum and then decreases with the shearing time, because the generation rate of new clusters slows down with time and d_f increases, i.e., the clusters become more and more compact. In the range of $3\% < \phi < 5\%$, the system evolves with the shearing time from the fluid of clusters to the Wigner glass of clusters in the end. In this ϕ range, the final conversion can reach $x = 80\%$ but further increase needs extremely long time. For $\phi > 5\%$, the system covers all the three phases and ends with a gel. As indicated by the two broken lines in Fig. 3, the glass state occurs in a large range of the cluster

packing fraction, $0.48 < \phi_c < 0.72$. This is related to the irregular shape and polydispersity of the clusters. A polydisperse system would lead to a wider range of glass transition compared with a monodisperse system.[38]

Fig. 5 shows the effective volume fraction of the primary particles forming the clusters, ϕ_e ($= x\phi$), as a function of ϕ along the phase evolution. The two broken lines represent the two transitions between Fluid and Glass and between Glass and Gel, respectively. It should be emphasised that since we are discussing the phase evolution along the shear-driven aggregation, Fig. 5 should not be considered as a phase diagram at the steady state of the shear-driven process, and each point in the diagram is associated with a set of values for ϕ, $\dot{\gamma}$, x, R_g and d_f at a specific time. It is seen from Fig. 5 that the ϕ_e range for the glass phase increases as ϕ increases. This is mainly due to the position of the Glass-Gel transition line, which increases with ϕ substantially. This is related to the average size of the clusters at the transition, which was found experimentally decreasing with ϕ, while the fractal dimension was practically identical ($d_f = 2.65 \pm 0.04$). It is known that if the fractal dimension is the same, the smaller is the cluster size, the higher the particle density within the cluster,[39] and it follows that the ϕ_e value at the transition increases as ϕ increases. To explain why the cluster size at the Glass-Gel transition decreases with ϕ, we recall that the percolation to gelation occurs only after the MC, and within the MC, the system has to be a fluid due to the extremely high shear. Then, as ϕ increases, in order for the system to be a fluid, the cluster size within the MC has to decrease. In Fig. 5, no phase transition data are reported for $\phi > 12\%$, because in this range the shear-driven gelation occurs after the system passes through the MC just one time. Thus, all the phase transitions occur within the residence time of the MC.

3.3 Construction of a steady-state phase diagram for the shear-driven process

The phase diagram in Fig. 5 is related to the dynamic evolution of the shear-driven process, out of the aggregation steady state. In fact, the conversion values are all far from $x = 1$. However, there is one point, P, which is the intersection of the glass and gel transition lines, and, not coincidently, P is located on the $x = 1$ line. This means that the system corresponding to Point P is at the steady state. However, P is difficult to reach experimentally because of the finite shearing time. On the other hand, it is true from the experimental data in Fig. 5 that all the systems with the ϕ values smaller than that at P, ϕ_p, would never reach the Wigner glass or gel phase, while those with $\phi > \phi_P$ would sooner or later become a Wigner glass and then a gel phase. Thus, the existence of Point P is confirmed. Of course, Point P varies with systems and shear forces, i.e., with colloidal interactions and Peclet number ($Pe = 3\pi\mu\dot{\gamma}a^3 / k_B T$). However, for a given Pe, a steady-state phase transition diagram may be drawn based on Point P.

To construct such a phase diagram, we note that Pe affects both the aggregation and breakage, resulting in the steady-state cluster size and structure. Thus, the crucial quantity that governs the steady-state cluster morphology is the difference between the energy barriers for aggregation (U_a) and breakage (U_b), $\Delta U = U_a - U_b$, as illustrated in the insert of Fig. 6. It follows that the phase diagram can be defined in the $\Delta U / k_B T$ vs ϕ plane, as shown in Fig. 6. The Wigner glass line is basically the trajectory of Point P discussed above, which divides the plane into fluids of clusters and solid-like gels. Increasing ΔU means increasing the aggregation barrier or decreasing the breakage barrier, thus favouring the breakage, and the steady-state cluster size decreases. Since at a fixed d_f, the smaller is the cluster, the higher the particle density within the cluster,[39] more primary particles are required to reach the Wigner glass state; it

follows that the Wigner glass line moves upward to a larger ϕ value. When ΔU increases to

reach a certain critical value, the cluster size reduces to the minimum, i.e., the size of a primary

particle; this means that within the MC, the breakage event is so strong that the effective

aggregation does not occur. An obvious case that corresponds to such a situation is when $U_b = 0$

($\Delta U = U_a$), as indicated in Fig. 6. Therefore, at the critical point, the line of the Wigner glass of

clusters will coincides with the repulsive glass of particles under stagnant conditions at $\phi \approx 0.58$.

This applies also to even larger ΔU values; thus, the line of the repulsive glass of particles in

this region is vertical. It should be pointed out that in the region of high ϕ values, i.e., on the

right hand side of the vertical broken line in Fig. 6, since the particles are already crowded, the

interparticle distance may become smaller than the position of the interaction energy maximum,

i.e., the particles become attractive. Thus, in this region, different arrested dynamics may occur

without shearing, such as attractive glass, dense packing, crystal, etc.

Of course, changing Pe will change the glass transition line in Fig. 6. However, since Pe

affects the aggregation and breakage in rather different kinetics, it is difficult to rationalize how

the position and shape of the glass transition line vary with Pe. On the other hand, no matter

how the systems are different and the Pe value varies, the principle of the phase diagram

presented in Fig. 6 has its general validity.

4. Concluding remarks

We have investigated in this work the phase evolution along the shear-driven aggregation

process of a polystyrene colloid in the range of the particle volume fraction, $\phi \in [2\%, 15\%]$,

through a microchannel (MC). Since the MC is very short (5.8 mm), the short residence time

allows us to snapshot the phase evolution by repeatedly cycling the aggregating system in the MC many times. An important feature of the system is that due to the strong repulsion between the particles generated by charges from the surface fixed charge groups and the adsorbed surfactants, the formed clusters are strongly repulsive as well, thus stable after shearing.

It is found that as the aggregation extent (thus, the cluster packing fraction) increases with the shearing time, depending on the initial particle volume fraction, we have progressively observed three phases: fluid of clusters, Wigner glass of clusters and gel. The presence of the Wigner glass state is obviously related to the repulsive nature of the system, which remains even after forming clusters. Along the shear-driven aggregation, the Wigner glass of clusters can occur in a large range of the packing fraction of total clusters ($0.48 < \phi_c < 0.72$), mostly due to the irregular shape of the clusters.

We have proposed a phase diagram that describes how the transitions of the three phases evolve at the aggregation steady-state in the colloidal interactions vs particle concentration plane. It tells that, as the difference between the aggregation and breakage energy barriers increases, the particle concentration for the occurrence of the Wigner glass of clusters increases. Therefore, the energy barriers for the aggregation and breakage, together with the particle concentration and the shear rate, determine the final clustered state. This scenario brings a clear understanding of the complicated shear-driven aggregation and solidification process and it is of great importance in applications.

Acknowledgment

References

1. P. J. Lu and D. A. Weitz, *Annu. Rev. Condens. Matter Phys.*, 2013, **4**, 217-233.

2. J. Bosse and S. D. Wilke, *Phys. Rev. Lett.*, 1998, **80**, 1260-1263.

3. D. Bonn, H. Tanaka, G. Wegdam, H. Kellay and J. Meunier, *Europhys. Lett.*, 1999, **45**, 52.

4. S. M. Underwood, J. R. Taylor and W. van Megen, *Langmuir*, 1994, **10**, 3550-3554.

5. W. van Megen and S. M. Underwood, *Phys. Rev. E*, 1994, **49**, 4206.

6. E. Zaccarelli, *J. Phys.-Condes. Matter*, 2007, **19**, 323101

7. A. Zaccone, J. J. Crassous and M. Ballauff, *J. Chem. Phys.*, 2013, **138**, 104908

8. N. Kovalchuk, V. Starov, P. Langston and N. Hilal, *Adv. Colloid Interface Sci.*, 2009, **147-48**, 144-154.

9. F. Sciortino, S. Mossa, E. Zaccarelli and P. Tartaglia, *Phys. Rev. Lett.*, 2004, **93**, 055701

10. P. N. Segrè, V. Prasad, A. B. Schofield and D. A. Weitz, *Phys. Rev. Lett.*, 2001, **86**, 6042.

11. W. Vanmegen and S. M. Underwood, *Phys. Rev. Lett.*, 1993, **70**, 2766-2769.

12. C. N. Likos, *Phys. Rep.-Rev. Sec. Phys. Lett.*, 2001, **348**, 267-439.

13. S. R. Williams and W. van Megen, *Stat. Phys.*, 2000, **519**, 3-10.

14. A. I. Campbell, V. J. Anderson, J. S. van Duijneveldt and P. Bartlett, *Phys. Rev. Lett.*, 2005, **94**, 208301.

15. A. Stradner, H. Sedgwick, F. Cardinaux, W. C. K. Poon, S. U. Egelhaaf and P. Schurtenberger, *Nature*, 2004, **432**, 492.

16. J. C. F. Toledano, F. Sciortino and E. Zaccarelli, *Soft Matter*, 2009, **5**, 2390-2398.

17. C. L. Klix, C. P. Royall and H. Tanaka, *Phys. Rev. Lett.*, 2010, **104**, 165702.

18. K. Kroy, M. E. Cates and W. C. K. Poon, *Phys. Rev. Lett.*, 2004, **92**, 148302.

19. A. Zaccone, H. Wu, D. Gentili and M. Morbidelli, *Phys. Rev. E*, 2009, **80**, 051404.

20.   J. Guery, E. Bertrand, C. Rouzeau, P. Levitz, D. A. Weitz and J. Bibette, *Phys. Rev. Lett.*, 2006, **96**, 198301.

21.   H. Wu, A. Tsoutsoura, M. Lattuada, A. Zaccone and M. Morbidelli, *Langmuir*, 2010, **26**, 2761-2768.

22.   H. Wu, A. Zaccone, A. Tsoutsoura, M. Lattuada and M. Morbidelli, *Langmuir*, 2009, **25**, 4715-4723.

23.   D. L. Xie, P. Arosio, H. Wu and M. Morbidelli, *Langmuir*, 2011, **27**, 7168-7175.

24.   D. L. Xie, A. Lamprou, G. Storti, M. Morbidelli and H. Wu, *Phys. Chem. Chem. Phys.*, 2012, **14**, 14374-14382.

25.   D. L. Xie, H. Wu, A. Zaccone, L. Braun, H. Q. Chen and M. Morbidelli, *Soft Matter*, 2010, **6**, 2692-2698.

26.   A. Zaccone, D. Gentili, H. Wu and M. Morbidelli, *J. Chem. Phys.*, 2010, **132**, 134903.

27.   A. Zaccone, D. Gentili, H. Wu, M. Morbidelli and E. Del Gado, *Phys. Rev. Lett.*, 2011, **106**, 138301.

28.   H. Wu, J. J. Xie, M. Lattuada and M. Morbidelli, *Langmuir*, 2005, **21**, 3291-3295.

29.   A. Zaccone, H. Wu and E. Del Gado, *Phys. Rev. Lett.*, 2009, **103**, 208301-208304.

30.   A. Zaccone, M. Soos, M. Lattuada, H. Wu, M. U. Babler and M. Morbidelli, *Phys. Rev. E*, 2009, **79**, 061401.

31.   Y. M. Harshe, M. Lattuada and M. Soos, *Langmuir*, 2011, **27**, 5739-5752.

32.   M. Soos, L. Ehrl, M. U. Babler and M. Morbidelli, *Langmuir*, 2010, **26**, 10-18.

33.   A. S. Moussa, M. Soos, J. Sefcik and M. Morbidelli, *Langmuir*, 2007, **23**, 1664-1673.

34.   L. Gmachowski, *Colloid Surf. A-Physicochem. Eng. Asp.*, 2002, **201**, 41-46.

35.   L. Ehrl, M. Soos and M. Lattuada, *J. Phys. Chem. B*, 2009, **113**, 10587-10599.

36. F. d. r. Cardinaux, E. Zaccarelli, A. Stradner, S. Bucciarelli, B. Farago, S. U. Egelhaaf, F. Sciortino and P. Schurtenberger, *J. Phys. Chem. B*, 2011, **115**, 7227-7237.

37. E. Zaccarelli and W. C. K. Poon, *Proc. Natl. Acad. Sci. U. S. A.*, 2009, **106**, 15203-15208.

38. G. L. Hunter and E. R. Weeks, *Rep. Prog. Phys.*, 2012, **75**, 066501

39. M. Lattuada, H. Wu and M. Morbidelli, *Langmuir*, 2004, **20**, 4355-4362.
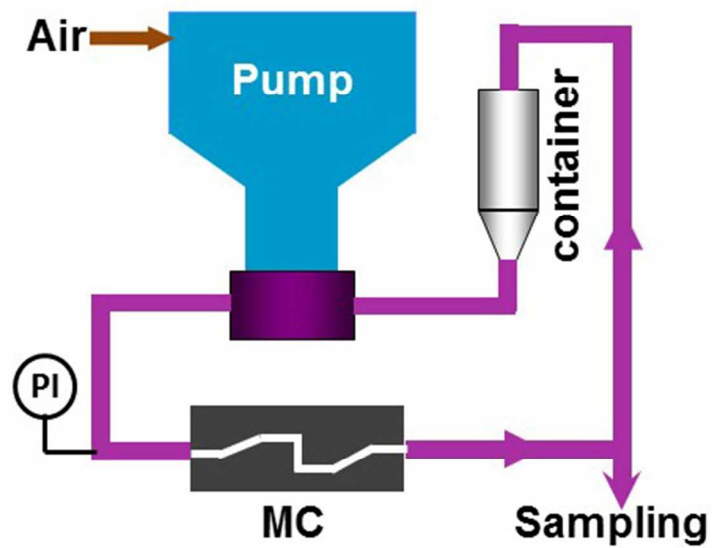
Sketch 1 The microchannel system for the shear-driven aggregation experiments, based on the commercial device, Homogenizer HC-5000 (Microfluidics, USA), equipped with a z-shape microchannel (MC) of a rectangular cross section.

Fig. 1
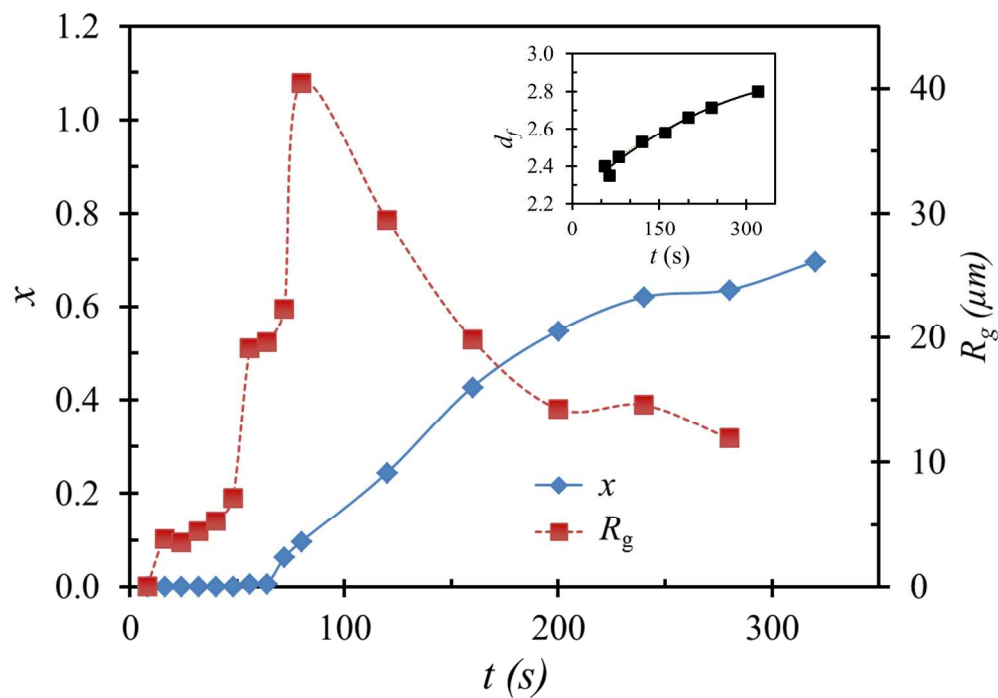
Fig. 1 Time evolution of the conversion (x) of the primary particles to big clusters and the average radius of gyration (R_g) of the big clusters, after shearing at $\dot{\gamma} = 1.5 \times 10^6 \text{ s}^{-1}$, in the case of $\phi = 3.0\%$. Inset: the corresponding time evolution of the fractal dimension (d_f) of the big clusters.

Fig. 2
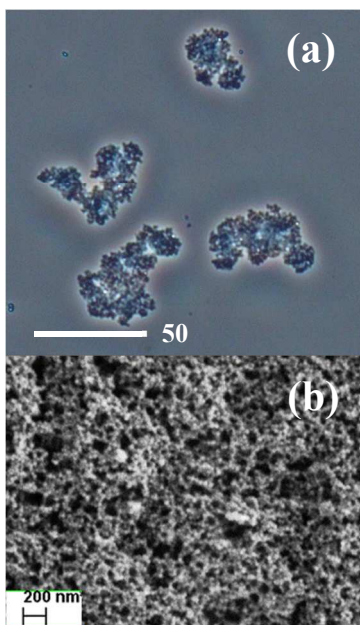
Fig. 2 Typical shape (a) and detailed structure (b) of the big clusters generated by the MC, characterized by an optical microscope and an scanning electron microscope, respectively.

Fig. 3
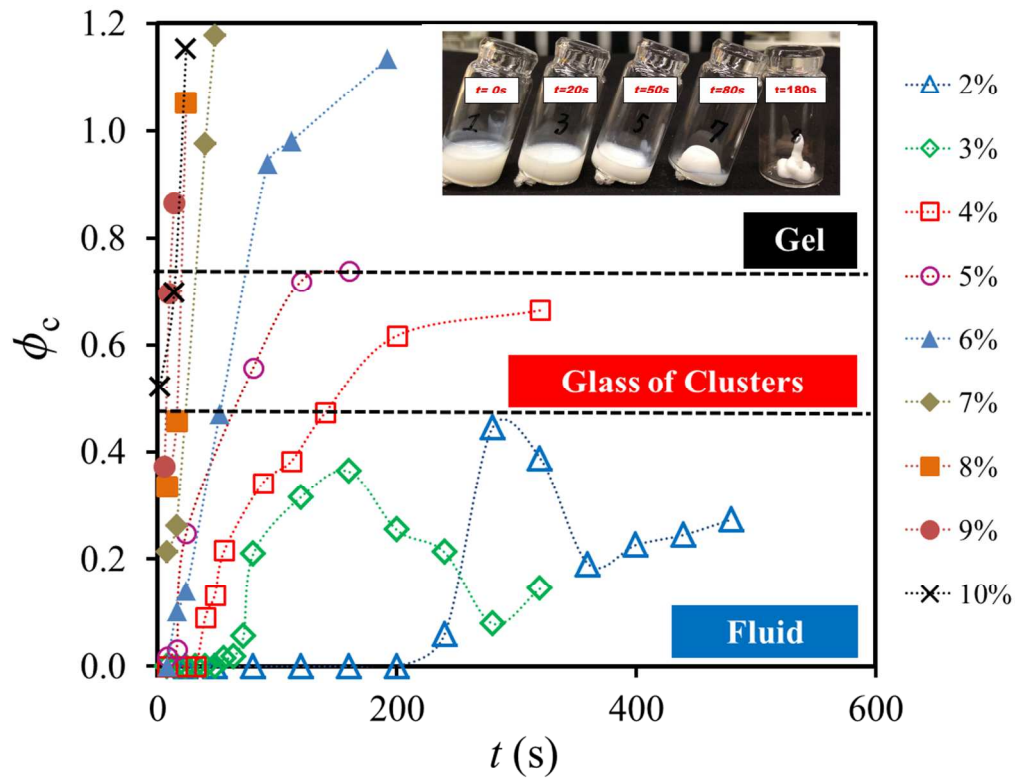
Fig. 3 Time evolution of the packing fraction of total big clusters (ϕ_c), after shearing at $\dot{\gamma} = 1.5 \times 10^6$ s^{-1}, at various values of the initial particle volume fractions (ϕ). Insets: pictures of the colloidal system after shearing for different times in the case of $\phi = 5.0\%$.
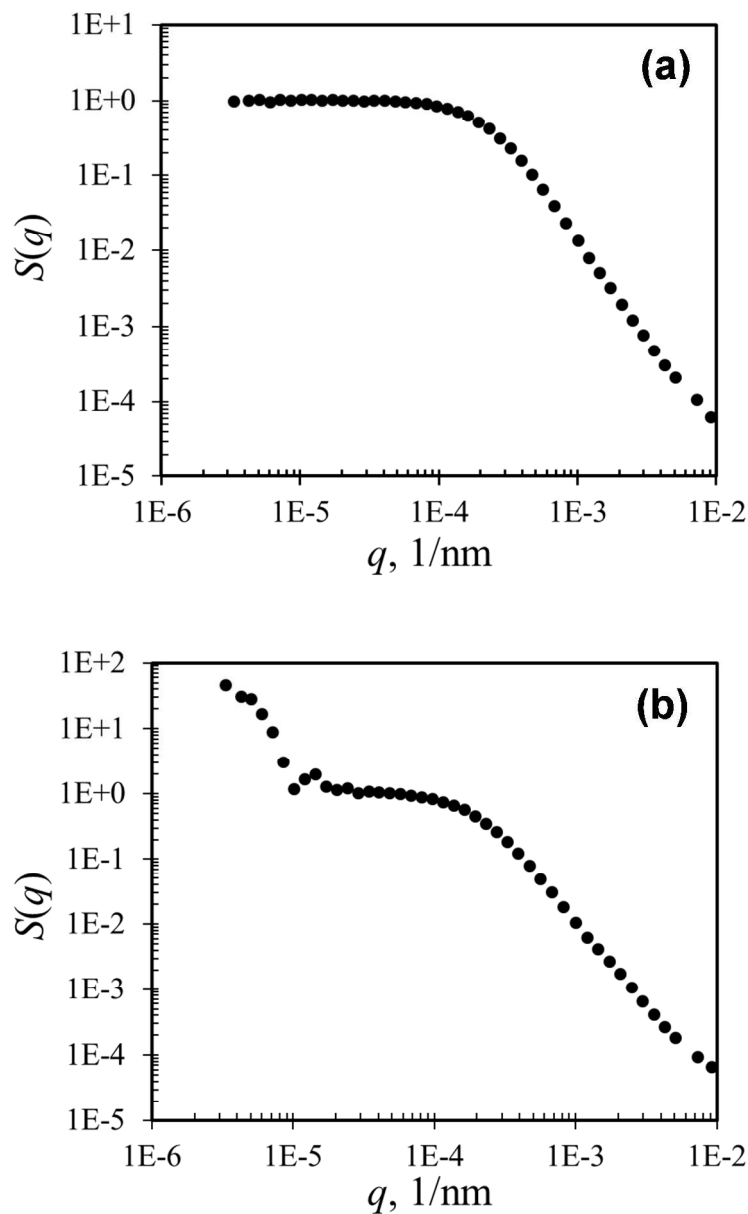
Fig. 4

Fig. 4 The scattering structure factor of the clusters, $S(q)$, which is obtained by dividing the measured intensity curve, $I(q)$, with the measured form factor of the primary particles, $P(q)$: (a) after dilution from a glass state at shearing time of 80 s and (b) after mechanical dispersion from a gel state at shearing time of 150 s. $\dot{\gamma} = 1.5 \times 10^6 \text{ s}^{-1}$; $\phi = 5.0\%$.
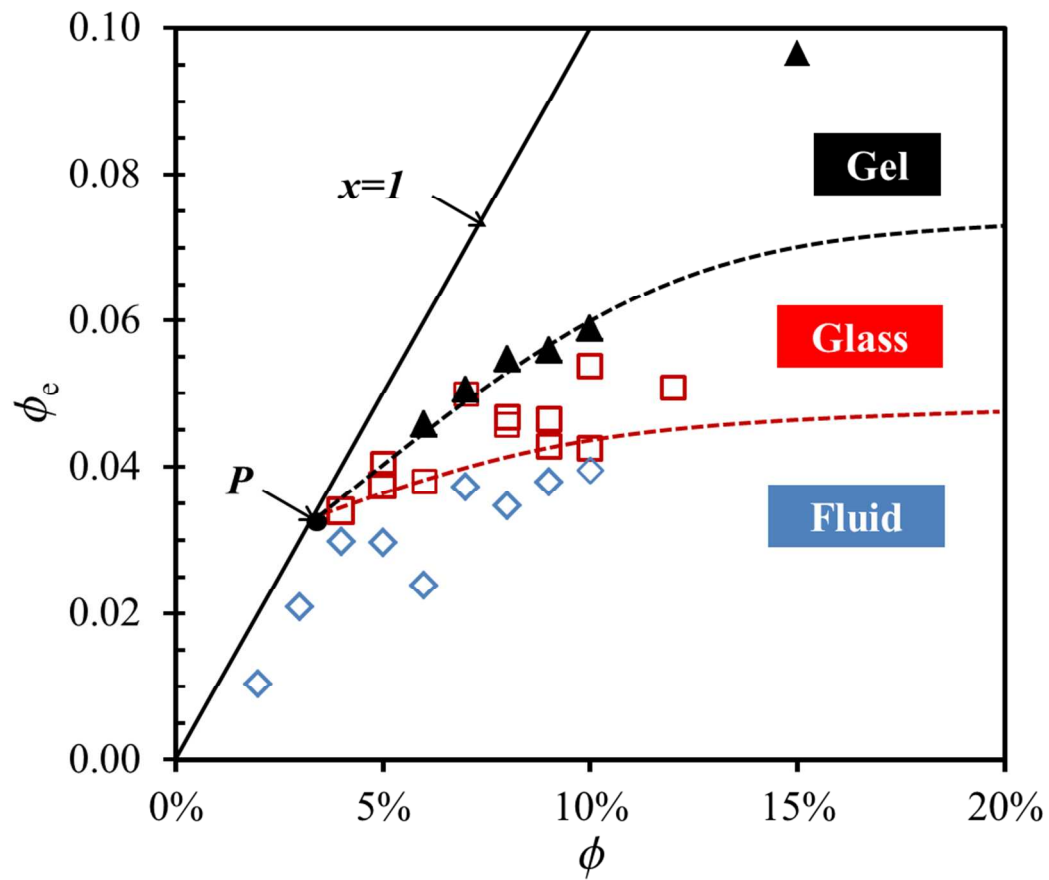
Fig. 5

Fig. 5 Phase evolution diagram along the conversion of the primary particles to big clusters at different initial particle volume fractions, displayed in the plane of the effective particle volume fraction to the big clusters ($\phi_e = x\phi$) vs the initial particle volume fraction (ϕ).
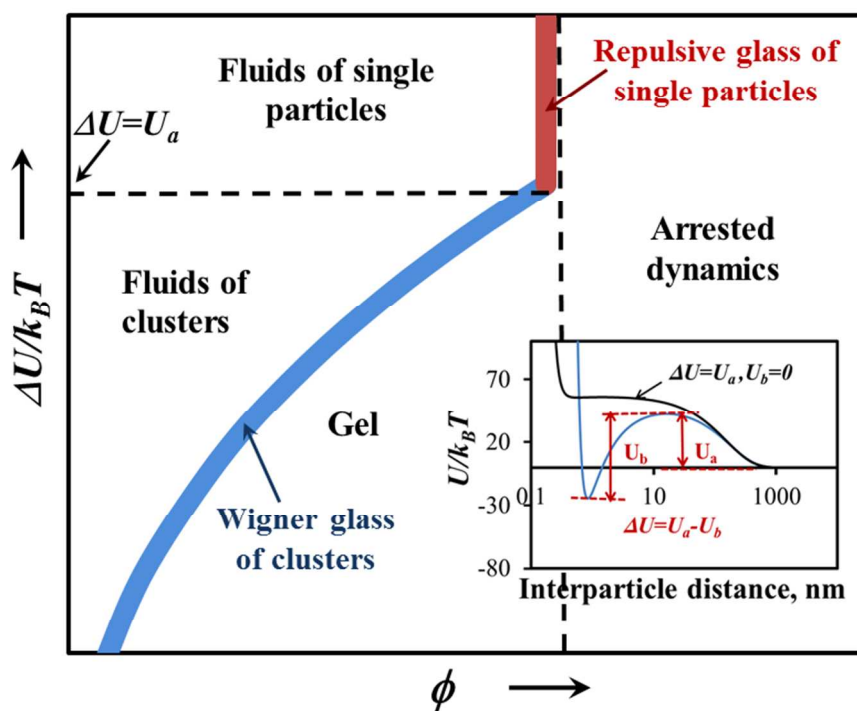
Soft Matter

Fig. 6

Fig. 6 Phase diagram at the steady state of the shear-driven aggregation process, presented in the plane of the difference between the aggregation and breakage energy barriers vs the initial particle volume fraction (i.e., $\Delta U / k_B T$ vs ϕ, where $\Delta U = U_a - U_b$), at a fixed Pe. Inset: illustration of the definition for the aggregation and breakage energy barriers related to colloidal interactions.

The table of contents entry

for

Snapshotted glass and gel transitions of stable colloidal dispersions after shear-driven aggregation in a microchannel

Xia Meng, Hua Wu* and Massimo Morbidelli*
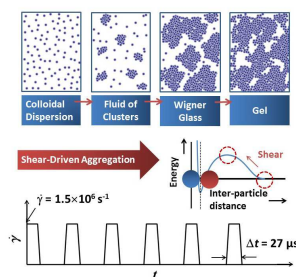
Along the shear-driven aggregation of strongly repulsive colloids, we have observed three phases: fluid of clusters, Wigner glass of clusters and gel.